

Low-Cost Adsorbent Development: Sulfuric Acid-Activated Teak Sawdust for Effective Methylene Blue Removal

Anselmus Boy Baunsele^{1*}, Hildegardis Missa², Dwi Siswanta³, Johnson N. Naat⁴, Yantus A. B. Neolaka⁴, Fidelis Nitti⁵, Abner Tonu Lema⁶, Rahmat Basuki⁷, Rahayu⁸

¹Chemistry Education Department, Faculty of Education and Teachers Training, Widya Mandira Catholic University, Kupang, East Nusa Tenggara, 85001, Indonesia

²Biology Education Department, Faculty of Education and Teachers Training, Widya Mandira Catholic University, Kupang, East Nusa Tenggara, 85001, Indonesia

³Department of Chemistry, Faculty of Mathematics and Natural Sciences, Gadjah Mada University, Yogyakarta, 55281, Indonesia

⁴Chemistry Education Department, Faculty of Education and Teachers Training, University of Nusa Cendana, Kupang, East Nusa Tenggara, 85001, Indonesia

⁵Department of Chemistry, Faculty of Mathematics and Natural Sciences, University of Nusa Cendana, Kupang, East Nusa Tenggara, 85001, Indonesia

⁶State Agricultural Polytechnic, Kupang, East Nusa Tenggara, 85001, Indonesia

⁷Department of Chemistry, Republic of Indonesia Defense University, Bogor, 16810, Indonesia

⁸Department of Chemistry, Faculty of Mathematics and Natural Sciences, University of Pattimura, Ambon, 97233, Indonesia

*Email: boybaunsele@gmail.com

Article Info

Received: Sep 24, 2024
Revised: Oct 22, 2024
Accepted: Nov 29, 2024
Online: Dec 16, 2024

Citation:

Baunsele, A. B., Missa, H., Siswanta, D., Naat, J. N., Neolaka, Y. A. B., Nitti, F., Lema, A. T., Basuki, R., & Rahayu. (2024). Low-Cost Adsorbent Development: Sulfuric Acid-Activated Teak Sawdust for Effective Methylene Blue Removal. *Jurnal Kimia Valensi*, 10(2), 246-259.

Doi:
10.15408/jkv.v10i2.41425

Abstract

The expansion of the global textile industry has resulted in a decline in environmental quality. Environmental pollution resulting from textile dye waste may include heavy metals and dyes, which exhibit carcinogenic and mutagenic effects. Many studies have been done to reduce the harm of dyes. Extensive research has been undertaken to mitigate the detrimental effects of dyes. One cost-effective approach for managing dye pollution is the adsorption of methylene blue using sulfuric acid-activated teak sawdust. Teak wood sawdust, a byproduct of the furniture industry that is abundant and underutilized, contains active sites within its constituent compounds, including cellulose, hemicellulose, and lignin. This study was designed to determine the ability of teak sawdust to adsorb methylene blue. In this investigation, the biosorbent will be characterized using fourier transform infrared spectroscopy (FTIR), scanning electron microscopy (SEM) and scanning electron microscopy-energy dispersive X-ray (SEM-EDX) to analyze its active sites and surface morphology. Additionally, the study aimed to elucidate the impact of variation contact time, pH solution, and alteration in methylene blue concentration on the adsorption capacity for methylene blue, employing a UV-Vis spectrophotometer for measurement. The research results demonstrated that optimal adsorption occurred at a contact time of 30 minutes and a pH of 6, with the adsorption efficiency reaching 99.67% as a function of contact time. The kinetic study was modeled using a pseudo-second-order approach, with a kinetic constant of 79.71 g mg⁻¹ min⁻¹. The maximum adsorption capacity was 1.351 mg g⁻¹, the n value was 1, and the percentage of methylene blue adsorbed reached 99.88%.

Keywords: Adsorption, acid-activated, methylene blue, teak sawdust

1. INTRODUCTION

The growth in industrial activity positively affects human welfare by generating additional employment opportunities, which can enhance the overall quality of life ¹. Conversely, industrial activities can generate waste that poses a risk of environmental damage. This waste must be treated before being discharged into natural ecosystems. Pollutants from industrial waste often include dyes and heavy metals ². Heavy metals have a terrible impact on the environment, especially humans, because they are toxic, difficult to decompose, and bioaccumulative ³. Suppose there is bioaccumulation of heavy metals in the human body. In that case, it can cause various diseases, for example, damage to nerve tissue, mental disorders, multiple types of cancer, and even death ⁴. Besides heavy metals, dyes are pollutants often produced by the textile industry, especially at the fabric dyeing stage and the final processing of textile fibers ⁵.

The textile industry commonly employs a range of dyes, including aniline blue, alcian blue, methyl orange, rhodamine B, methylene blue, crystal violet, toluidine blue, and congo red ⁶. Dyes can precipitate various environmental issues, including a diminution in dissolved oxygen in aquatic systems, Decreasing the penetration of sunlight into marine environments and diminishing the photosynthetic activity of aquatic plants ⁷. Dyes are toxic and carcinogenic; by bioaccumulation, they can cause cancer and mutagenesis ⁸ and cause various problems such as vomiting, nerve damage, increased heart rate, and cyanosis ⁹. Dyes can form complex compounds when accumulated to increase the resistance to light and heat ¹⁰, and challenging to degrade chemically and biologically ¹¹. Dyes can be classified into anionic and cationic categories. Congo red is an example of a cationic dye employed in the textile industry. When such dyes accumulate in the human body, the azo group can be metabolized into benzidine, a compound identified as a significant carcinogen ¹². In addition to anionic dyes, methylene blue is a prominent cationic dye extensively used in textile applications. However, it is known to cause skin irritation and damage to ocular tissue ¹³, increase heart rate, nausea, and cyanosis, and affect the metabolism of nervous tissue¹⁴. The various effects of methylene blue were the reason to treat the dye became safer for the environment.

Numerous strategies have been developed to diminish the environmental impact of methylene blue waste. The methods that have been developed include photocatalytic methods using $\text{Fe}_3\text{O}_4/\text{ZnO}$ catalysts ¹⁵ and silver nanoparticles ¹⁶, electroflotation using TiO_2 catalyst ¹⁷, dye biodegradation using bacteria ⁸, electrochemical degradation utilizing carbon-PVC electrodes ¹⁸ and adsorption by adsorbent ¹⁹.

Adsorption is an easy method and low-cost to apply ²⁰. Adsorption is often used as an appropriate method for removing azo dyes because it is cheap and environmentally friendly ²¹. Agricultural and household waste has been widely used as an adsorbent, for example, lemongrass leaves ⁹, seaweed ²², papaya bark fiber ²³, sugarcane bagasse ²⁴, coconut fiber ²⁵⁻²⁹, palm fruit fiber ³⁰⁻³², tea waste ³³, clove leaves ³⁴, lime, date and eucalyptus sawdust ³⁵, mangrove sap ¹⁹, watermelon seed pulp ³⁶, peanut shells ³⁷ and teak sawdust ³⁸. However, these studies were conducted to assess the potential of new materials to be used as methylene blue adsorbents.

A variety of natural materials are used as adsorbents for methylene blue. Teak sawdust is an agricultural waste material that high potentially act as an adsorbent for pigment removal. This waste is abundant in Kupang City, especially in the furniture home industry, which is burned without treatment. Moreover, the large amount of sawdust waste was used as a dampening agent, raw material for concrete blocks and biomass for power generation ³⁹. Although the use of teak sawdust in the form of activated carbon is widely used as an adsorbent, the use of directly activated teak sawdust is still rarely found in the literature. The activated-teak sawdust can be activated to remove surface impurities and enhance its adsorption capacity for the target adsorbate ⁴⁰. The adsorbents can be activated using an essential activator ⁴¹ or acid ⁴². This work aims to evaluate the adsorption capacity of teak sawdust waste activated with sulfuric acid as methylene blue (MB) adsorbent. Sulfuric acid increases the porosity of the adsorbent and its adsorption capacity because it has a high ionization energy compared to other types of acids ⁴³. The adsorbate investigated in this study is MB ($\text{C}_{16}\text{H}_{18}\text{N}_3\text{SCl}$), which it is a widely used pigment to kill parasites and fungi in fish farming. Further, the adsorption study in this research includes determining kinetic and isothermal models.

2. RESEARCH METHODS

Materials and Tools

The substances employed in this experiment comprised teak sawdust (sourced from a furniture workshop in Kupang City, Indonesia), analytical-grade NaOH crystals (Merck KgaA, Darmstadt, Germany), 37% analytical-grade HCl, sulfuric acid (Merck KgaA, Darmstadt, Germany), deionized water, and methylene blue (Merck). The instruments used are a UV-Vis spectrophotometer (Thermos Scientific), a Fourier transform infrared spectrometer (Shimadzu IR Prestige 21), a scanning electron microscope-energy dispersive X-ray (JSM-6510LA), a pH meter (Mettler Toledo and PH-009 (I) A), an analytical balance (Meter AE 200 and Acis AD 300H), a magnetic stirrer and an oven.

Adsorbent Preparation

Teak wood sawdust from the furniture is washed using water to remove the impurities, then grind it using a mortar. The teak sawdust powder is then sieved using an 80 Mesh sieve. The sifted powder was subsequently rinsed with distilled water and dehydrated at 80°C for four hours. The dehydrated material was submerged in 1 liter of 0.05 M sulfuric acid solution and agitated for 4 hours⁴¹, then rinsed with distilled water until the pH reached neutrality. Acid activation is intended to eliminate impurities from the adsorbent and may enhance its adsorption capacity⁴⁴. The teak sawdust activated by sulfuric acid (TSAA) can be used as an adsorbent for methylene blue adsorption.

Characterization

The characterization of the TSAA biosorbent was performed using scanning electron microscopy (SEM) and scanning electron microscopy-energy dispersive X-ray (SEM-EDX), Fourier-transform infrared spectroscopy (FTIR), and point of zero charge (pH_{zpc}) analysis. FTIR is employed to detect the functional groups existing in the TSAA biosorbent⁴⁵, for the FTIR analysis, solid samples are crushed and mixed with KBr pellets, then placed in the FTIR instrument and irradiated in the infrared. Vibrations generated by functional groups in the material are detected to provide molecular information about the material. Whereas scanning electron microscopy is utilized to analyze the biosorbent surface morphology⁴⁶. The SEM and SEM-EDX are analyzed by inserting the sample into the instrument and scanning to obtain the surface morphology and the distribution of atoms or elements on the adsorbent surface. Moreover, the characterization of biosorbents is also carried out to determine the pH zero point charge (pH_{zpc}). The pH_{zpc} was determined by preparing eight containers containing 20 mL of 0.1 M NaCl solution. The pH of these solutions was adjusted to values spanning from 3 to 10 using NaOH and HCl. A total of 0.1 g of TSAA was put into each container, stirred for 30 minutes, then left for 24 hours. After 24 hours, the final pH of the solution in each container was recorded. The pH_{zpc} was determined by plotting a curve of the initial pH (pH_i) against the divergence between the primary pH and the final pH (ΔpH). The pH_{zpc} value is identified as the point where pH_i equals ΔpH⁴⁷.

The Adsorption Optimization

pH effect analysis is performed by preparing a quantity of 100 mg of MB powder was dissolved in 1000 mL of distilled water, producing 100 parts per million (ppm) MB solution. The maximum wavelength is then determined by diluting the standard

MB solution to a concentration of 5 ppm. The solution's maximum peak absorption was retrieved at 600 and 700 nm wavelengths using a UV-Vis spectrophotometer. Subsequently, the calibration curve was developed by preparing MB stock solution dilutions to achieve concentrations of 2, 4, 6, 8, and 10 ppm and analyzing the absorption at the previously determined maximum wavelength. The absorbance data are employed to derive the linear equation. Eight containers were prepared, each with 20 mL of 10 ppm MB solution. The pH of the solutions was then adjusted to 3, 4, 5, 6, 7, 8, 9, and 10, respectively. Furthermore, 0.1 g of biosorbent was added into each batch and stirred for 75 minutes⁴⁸. After the stirring process, the filtrate was collected and analyzed using UV-Vis spectroscopy to identify the pH condition of the methylene blue (MB) solution that exhibited the highest adsorption capacity.

Time variation analysis was performed by preparing 8 containers, each containing 20 mL of 10 ppm MB solution, and the pH of each container was adjusted to the previously determined optimal value. 0.1 g of biosorbent was added to each container, and they were shaken with varying contact times of 5, 10, 20, 30, 45, 60, 75, and 90 minutes, respectively. The filtrate from each container was then measured using UV-Vis to determine the adsorption capacity at the different contact times. The absorbed MB on the biosorbent was calculated using Equation (1) to measure the percentage of MB absorbed and Equation (2) to measure the adsorption capacity.

$$\text{adsorption efficiency} = \frac{C_0 - C_e}{C_0} \times 100\% \quad (1)$$

$$q = \frac{(C_0 - C_t)v}{m} \quad (2)$$

where C_0 and C_e denote the concentration before and after adsorption. The concentration at a specific time is expressed as C_t , while v is the volume of MB solution and m is the mass of the teak sawdust biosorbent. Additionally, q refers to the adsorption capability of the adsorbate onto the adsorbent, expressed in mg g^{-1} ⁴⁹.

The data of variation contact time adsorption was then used to determine the kinetic value of the MB adsorption by the biosorbent. Analysis of adsorption kinetic data can be carried out using four adsorption kinetic models shown in **Table 1**. The R^2 value of the four kinetic models that is closest to one is the kinetics MB kinetic adsorption using TSAA biosorbent⁵⁰.

Investigations to determine how the solution concentration varies were carried out by preparing 8 containers, each containing 20 mL of MB solution at concentrations of 5, 10, 20, 30, 45, 50, 60, 70, and 90 ppm, respectively. Additionally, the pH of each container was adjusted to the optimal level for adsorption. Each container was supplemented with 0.1

g of 80-mesh biosorbent and subjected to shaking for the optimal contact time. Following this, the filtrate was analyzed using UV-Vis spectroscopy to ascertain the optimal adsorption concentration.

Data on the variations in MB concentration and maximum adsorption capacity were employed to evaluate the isothermal adsorption models for the

biosorbents. The adsorption isothermal models applied include Langmuir, Freundlich, Temkin, Harkin-Jura, Redlich-Peterson, Jovanovic, and Halsey models. The linear equation of these seven mathematical models can be determined by plotting the data available in **Table 2**.

Table 1. Kinetic models for MB adsorption with TSAA

Kinetic model	Linear form	Plot graph	Reference
PFO	$\ln(qe - qt) = \ln qe - kt$	t vs $\ln(qe - qt)$	51
PSO	$\frac{t}{qt} = \frac{1}{kqe^2} + \frac{t}{qe}$	t vs $\frac{t}{qt}$	51
Elovich	$qt = \left(\frac{1}{\beta}\right) \ln(\alpha\beta) + \left(\frac{1}{\beta}\right) \ln t$	qt vs $\ln t$	52
Intraparticle diffusion	$qt = kp\sqrt{t} + C$	qt vs \sqrt{t}	52

Table 2. Mathematical model for MB adsorption isothermal

Isothermal model	Linear regression	Plot graph	Parameter	Reference
Langmuir	$\frac{1}{qe} = \frac{1}{q_m} + \frac{1}{Klq_mCe}$	$\frac{1}{qe}$ vs $\frac{1}{Ce}$	$\frac{1}{q_m} = \text{intercept}$ $q_m = \frac{1}{\text{intercept}}$ $Kl = \frac{1}{q_m \times \text{slope}}$	53
Freundlich	$\log qe = \log Kf + \frac{1}{n} \log Ce$	Log qe vs log Ce	$n = \frac{1}{\text{Slope}}$ $Kf = e^{\text{intercept}}$	53
Temkin	$qe = \beta \ln K_T + B \ln Ce$	$\ln Ce$ vs qe	$A = e^{\frac{\text{intercept}}{B}}$ B = slope	54
Harkin-Jura	$\frac{1}{qe^2} = \frac{B}{A} - \left(\frac{1}{A}\right) \log Ce$	$\frac{1}{qe^2}$ vs $\log Ce$	$A = \frac{1}{\text{Slope}}$ $B = A \times \text{intercept}$	55
Redelich-Peterson	$\ln \frac{Ce}{qe} = \beta \ln Ce - \ln A$	$\ln \frac{Ce}{qe}$ vs $\ln Ce$	Kr = intercept $\beta = \text{slope}$	55
Jovanovic	$\ln qe = \ln q_{max} - K_j Ce$	$\ln qe$ vs Ce	$q_{max} = e^{\text{intercept}}$ $K_j = \text{slope}$	55
Halsey	$\ln qe = \frac{1}{n_H} \ln k_H - \left(\frac{1}{n_H}\right) \ln Ce$	$\ln Ce$ vs $\ln qe$	$n_H = \frac{1}{\text{slope}}$ $k_H = e^{\text{intercept}}$	56

3. RESULTS AND DISCUSSION

FTIR Analysis of TSAA

The TSAA biosorbent was analyzed using FTIR to recognize the functional groups existing in the material. Teak wood are known to contain hemicellulose, lignin and cellulose compounds ⁵⁷. Cellulose present in organic materials is recognized for its potential as an adsorbent for cationic dyes, including methylene blue ⁵⁸. FTIR analysis of TSAA biosorbent is shown in **Figure 1**.

The data depicted in **Figure 1** illustrates the Fourier-transform infrared (FTIR) spectrum for teak sawdust. The changes experienced by the TSAA material before activation, after activation and after adsorption of MB are shown in Figure 1. There are

changes in the peak of the spectrum showing a change in the intensity of the functional groups vibrations. These peaks at wave numbers 3426 and 3410 cm^{-1} are vibrations produced by the -OH group before and after MB adsorption. Since the conditions before and after the adsorption have the same vibrations, it is assumed that there are other components that are bound to the -OH functional group. The vibration indicated the present -OH alcohol or phenol compounds ⁵⁹. Vibrations that occur at wave numbers 2924 and 2940 cm^{-1} suggest the presence of the -CH group; this is because vibrations in the range of 2700 to 3300 cm^{-1} are the absorption area for the -CH functional group with a medium peak intensity ⁶⁰.

The observed peaks at wave numbers 2376, 2369, and 2338 cm^{-1} suggest vibrations attributable to the C=C or C=N functional groups ⁶¹. The peak observed at a wave number of 1736 cm^{-1} is indicative of a strong vibration associated with the C=O functional group ⁴⁵. The C=O group is indicated by vibrations at a wave number of 1512 cm^{-1} ²³. The peaks observed at wave numbers 1057 and 1034 cm^{-1} denote the presence of the C—O functional group, which is suspected to belong to alcohol and ether compounds

within cellulose molecules ⁶². The data illustrated in **Figure 1** demonstrates the variations in vibration intensity for each functional group in the biosorbent before and after MB adsorption. This occurs because the adsorption of MB induces changes in the molecular size on the adsorbent's surface, leading to modifications in the vibrational properties compared to those observed before adsorption. The functional groups observed in the teak sawdust biosorbent are similar to the research results in **Table 3**.

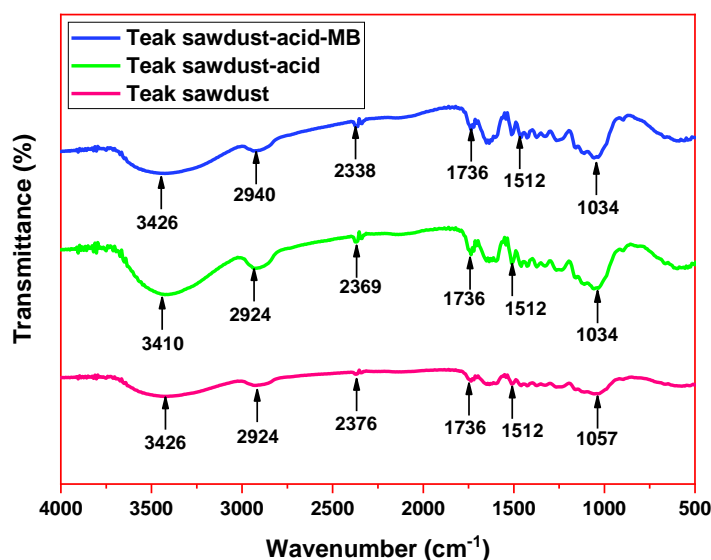


Figure 1. FTIR spectrum of the biosorbent prior to and following MB adsorption

Table 3. FTIR Analysis Results for Various Biosorbents

Functional groups	Wavenumber (cm^{-1})	Biosorbent
C—H; C=O; O—H	2910; 1740; 3400	Sugarcane bagasse ²⁴
C—H; C=O; O—H	2924–2933.7; 1730–1724; 3296	Tea waste ³³
C—H; C—C; O—H	2926 and 2930; 1423 and 1462; 3447 and 3412	Moringa oleifera seed pod ⁴⁷
C—H; C=O; O—H;	2900; 1700-1600; 3500-3100	Mushroom ⁶³
C—H; C—O; O—H; C=C	2939.52; 1267.23 and 1060.85; 3296.35; 1608.63 and 817.72	Coconut fiber ⁶⁴
C—H; C—O; O—H	2927; 1064; 3355	Chitosan ⁶⁵
C—H; C—O; O—H; C—C	1459 and 1377; 1744 and 1711; 3370; 2923 and 2854	Coconut pulp ⁶⁶
C—H; C—O; O—H; C—C; C=O	2918.53; 1162.2; 3433; 1629.99; 1431.02	Figs ⁶⁷
C—H; C=O; O—H; C=C	2926.01; 1705–1739.79; 3433.29; 1624.06–1618.28	Coconut husk ⁶⁸
C—H; C=O; O—H; C=C	2924 and 2940; 1512; 3426 and 3410; 2376, 2369 and 2338	This study

TSAA SEM Analysis

The surface morphology of teak sawdust was assessed through SEM and SEM-EDX analyses. The SEM images of the biosorbent at magnifications of 200x and 1000x, both before and following adsorption, are described in **Figure 2**. The SEM data reveal that the surface of TSAA exhibits small, oval-shaped particles. The greater the magnification obtained, the more visible the shafts on the surface of

the biosorbent ²³. **Figure 2** shows that after the adsorption process, there is a smooth fibre spread on the surface of the biosorbent. These data indicate that MB is adsorbed onto the surface of the biosorbent, resulting in a change in the surface morphology of the biosorbent and the morphological appearance of the biosorbent-like particles that are homogeneous and irregular in size.

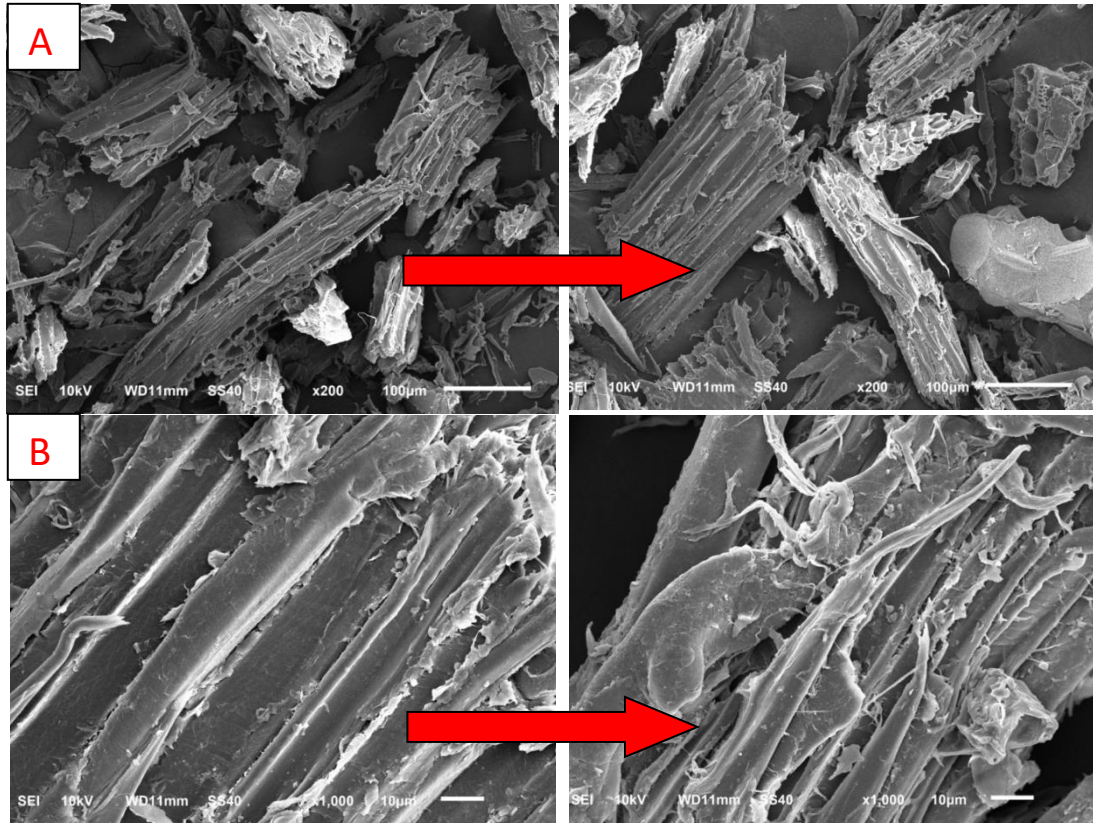


Figure 2. The SEM analysis before and after MB adsorption for magnification of, A) 200 times and B) 1000 times

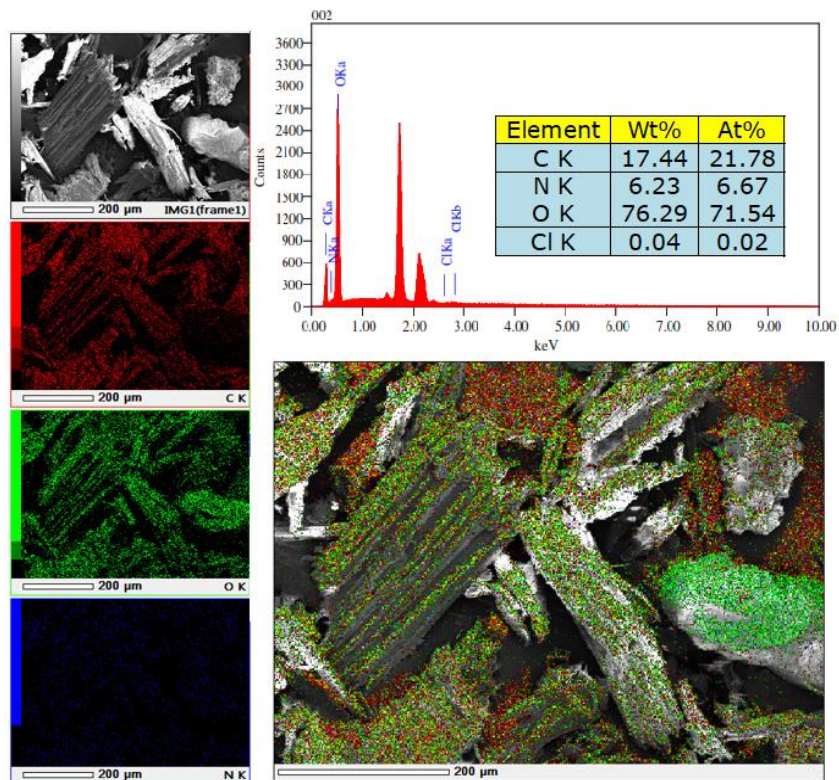


Figure 3. SEM–EDX analysis results

Figure 3 shows the results of SEM–EDX analysis of biosorbent after MB adsorption. SEM-EDX analysis identifies and maps the atom distribution from the adsorbate on the biosorbent's surface. The surface of the adsorbent is known to exhibit atomic mass percentages of C (17.44%), N (6.23%), O (76.29%), and Cl (0.04%). The detection of carbon (C) and oxygen (O) elements in the SEM-EDX analysis is attributed to the existence of C–O functional groups characteristic of alcohols, carboxylic acids, and esters. The presence of chlorine (Cl) observed in the EDX Mapping analysis suggests the adsorption of methylene blue (MB) compounds onto the biosorbent surface. The presence of nitrogen (N) highlights the existence of azo bonds (–N=N–), which function as chromophores and are a principal characteristic of dye compounds ⁴¹.

The pH_{pzc} analysis of TSAA

This analysis aims to determine the charge on the surface of the biosorbent. According to the data presented in **Figure 4**, the pH at which the biosorbent surface exhibits a net zero charge is determined to be pH 6. It's explained that when pH is 6, the opportunity for interaction between adsorbent and adsorbate will be higher because no competitors are blocking it ⁶⁹. When the pH is below the pH_{pzc} , the biosorbent surface acquires a positive charge, increasing its affinity for anions ⁷⁰. Conversely, a repulsion between the positively charged biosorbent and the cationic MB will arise. At pH levels exceeding the pH_{pzc} , the biosorbent surface acquires a negative charge, predisposing it to interact with cations ⁷¹.

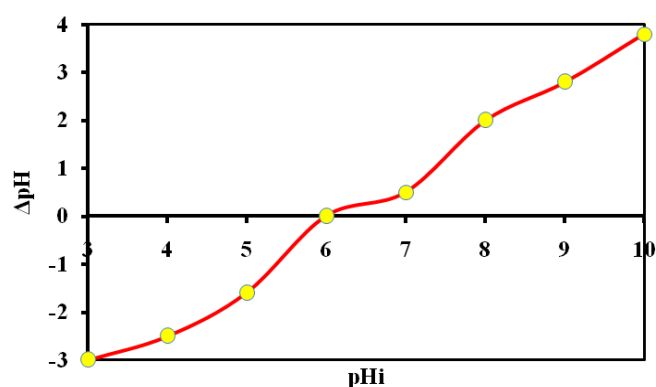


Figure 4. Biosorbent pH_{pzc} data

The effect of MB pH Variation

The adsorption study begins with determining the maximum wavelength of MB. The wavelength used in this research is 665 nm ⁴⁸. After obtaining the maximum wavelength, the linear equation was determined by plotting a graph of MB concentration versus absorbance. The data obtained was $y = 0,22x + 0,006$ with a value of $R^2 = 0,997$. The

linear equation obtained from the standard curve was then evaluated to investigate the impact of the pH of the MB solution on its adsorption capacity.

The MB adsorption test uses pH variations of the MB solution, presented in **Figure 5**; this indicates that the optimal adsorption is achieved at pH 6, where the adsorption capability reaches 1.96 mg g^{-1} and the adsorption efficiency is 99.35%. The data presented in **Figure 5** is corroborated by **Figure 4**, which shows that at pH 6, the biosorbent surface is neutral, eliminating any interfering ions that could affect the interaction between the active sites of MB and the biosorbent. This data can be explained by the fact that the MB solution has an acidity level below 6 or a $pH < 6$, H^+ ions and MB cations will compete in interactions with the negative partials on cellulose so that little adsorbate will be bound to the adsorbent. Whereas, if the MB solution has an acidity above 6 or $pH > 6$, the positive partial in the MB will be attacked by OH^- ions, thus preventing the MB from interacting with the negative partial in the biosorbent ¹⁹.

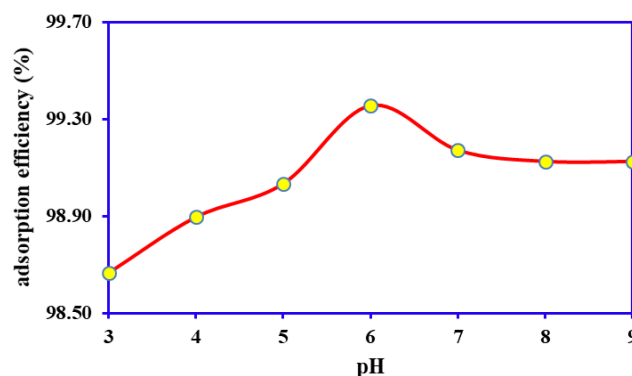


Figure 5. The effect pH of MB adsorption

Adsorption Kinetic

The optimum contact time is when the adsorption process attains its optimal capacity for adsorbate uptake. The data presented in **Figure 6** indicates that the optimal contact time for adsorption is 30 minutes, corresponding to an adsorption capacity (qt) of 1.968 mg g^{-1} , and the adsorption efficiency reaches 99.67%. The data presented in **Figure 6** reveals that the sorption capacity of MB using the biosorbent increases progressively from 5 to 30 minutes. This phenomenon is attributed to the functional area on the biosorbent surface, which promotes the adsorption process. At 30 minutes, optimum MB adsorption conditions were achieved. After 30 minutes of adsorption, it will tend to occur constantly because there is a possibility that the active site of the biosorbent has been filled by the adsorbate so that there are no new interactions between the biosorbent and the adsorbate. When optimum adsorption conditions were achieved, it was found that the TSAA biosorbent was able to remove 99.67% of MB.

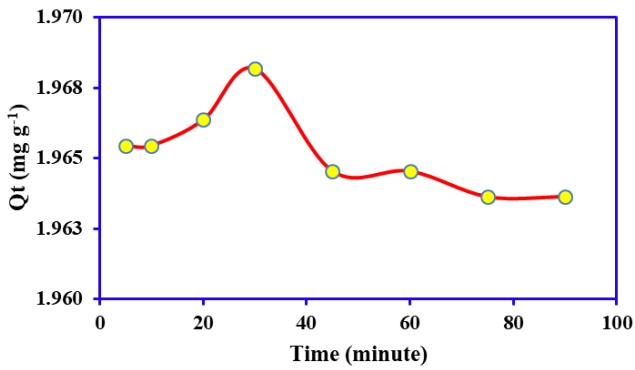


Figure 6. Influence of variation time on methylene blue adsorption

Table 4. Kinetic parameters of MB adsorption by TSAA

Models	Kinetic parameters
Pseudo first order	K_1 ($0.0000004 \text{ min}^{-1}$)
	Q_e (18.52 mg g^{-1})
	R^2 (0.7)
Pseudo second order	K_2 (79.71 min^{-1})
	Q_e (2.004 g mg^{-1})
	R^2 (1)
Elovich	β (0.0032 g mg^{-1})
	α ($2414.9 \text{ mg g}^{-1} \text{ min}^{-1}$)
	R^2 (0,533)
Intraparticle diffusion	K_p (896.6)
	C (1826)
	R^2 (0.253)

According to the data provided in **Table 4**, it is known that the R^2 value for the pseudo-second-order adsorption kinetics model is the closest to one among the four mathematical models. This data indicates that

the methylene blue (MB) adsorption rate is influenced by both the quantity of the adsorbate and the availability of binding area on the surface of the adsorbent. The measured MB sorption capacity of the biosorbent, which is 18.52 mg g^{-1} , is comparable to the 2.004 mg g^{-1} derived from the maximum adsorption capacity calculated using the pseudo-second-order kinetic model, explained in **Figure 7**. The adsorption process demonstrates that the quantity of available functional area influences the adsorption capacity on the adsorbent surface. Based on the data in **Figure 6**, the decrease in adsorption capacity is suspected because the interaction between the adsorbate and the active site on the adsorbent is weak, so that desorption tends to occur. This methylene blue adsorption kinetics data is similar to several biosorbent studies for dye adsorption, which occurs according to pseudo-second-order kinetics, as shown in **Table 5**.

Table 5. MB adsorption kinetics data by several biosorbents

Biosorbent	Adsorbate	R^2
Coconut fiber ⁷²	Methylene blue	1
Mangrove plant sap ¹⁹	Methylene blue	0.999
Coconut fiber ⁷⁰	Rhodamine B	0.987
Moringa skin fruit ⁴⁷	Rhodamine B	0.999
Sugarcane bagasse ⁷³	Methylene blue	0.999
Eucalyptus sawdust ³⁵	Methylene blue	0.999
Chinar leaves ⁷⁴	Methylene blue	1
Dry lear litter ⁷⁵	Methylene blue	0.99
Coconut bunch ⁷⁶	Methylene blue	0.99
Clove leaves ⁴¹	Methylene blue	0.99
Lemongrass ⁹	Methylene blue	0.97

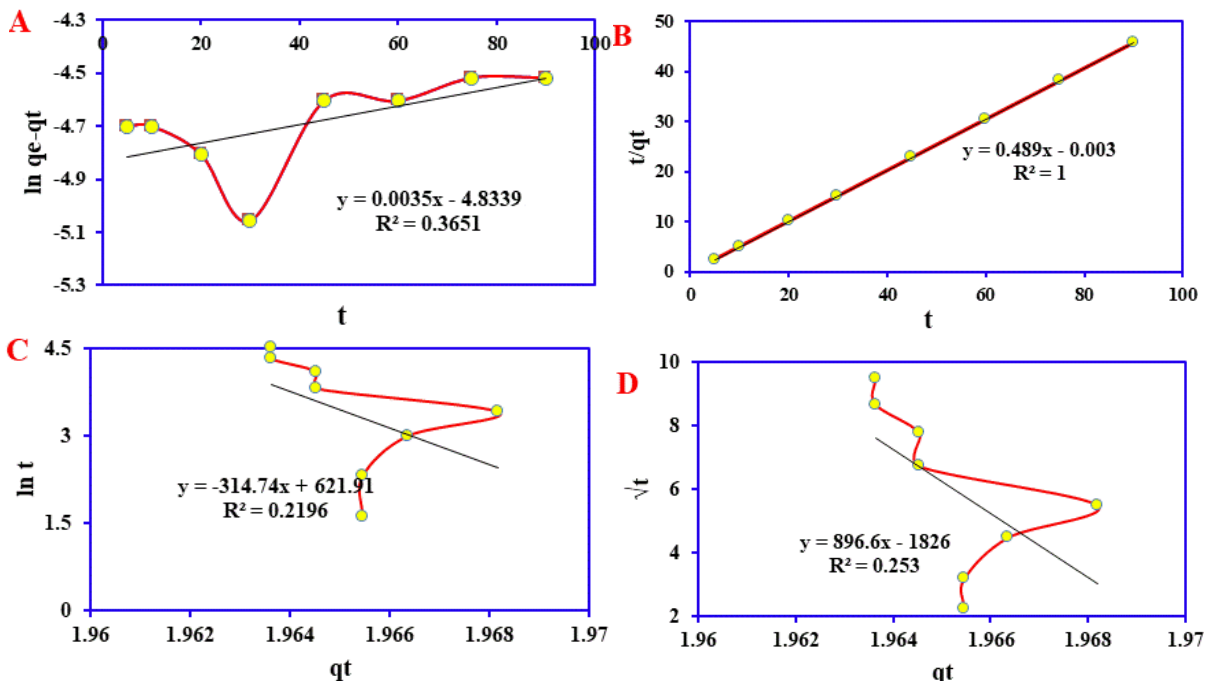


Figure 7. Adsorption kinetic model graph, A) PFO; B) PSO; C) Elovich; 4) Intraparticle diffusion

Adsorption Isothermal

The adsorption process initiates with the adsorptive migrating to the adsorbent surface. Once the adsorbate reaches the surface of the adsorbent, interactions may occur between the adsorbent's active sites and the adsorbate, facilitating the adsorption of the adsorbate into the pores of the adsorbent¹⁴. The impact of varying MB concentrations on adsorption was investigated by adjusting MB concentrations between 5 and 90 ppm. The adsorption experiments were conducted at a contact time of 30 minutes and pH 6. The data presented in **Figure 8** demonstrates that the highest adsorption capacity for the adsorbate is achieved at a concentration of 45 ppm, with an adsorption efficiency of 99.88%. It can be inferred that within the 5 to 30 ppm concentration range, the adsorption percentage is expected to increase due to numerous reactive sites on the biosorbent, which can facilitate the binding of MB. Under these conditions, the amount of binding sites on the biosorbent exceeds that of the MB molecules. At concentrations greater than 45 ppm, there is a decrease in adsorption capacity because a layer of MB already covers the active site of TSAA, and no further adsorption process occurs because the adsorbent has reached a saturated condition⁴⁵. MB isothermal adsorption was investigated using seven isothermal models, as detailed in **Table 2**. The correlation coefficients for each isothermal model were determined through linear regression analysis. The isothermal parameter values are provided in **Table 6**, and the linear regression plots are illustrated in **Figure 9**. According to **Table 6**, the isothermal model that exhibits an R^2 value closest to 1 is the model describing the adsorption of MB onto TSAA.

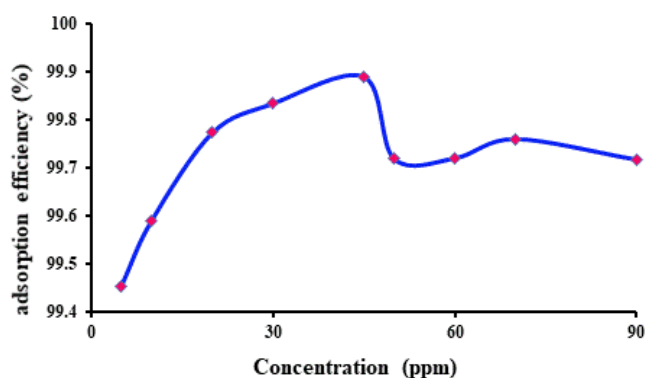


Figure 8. Effect of initial concentration of MB

Table 6. Isothermal adsorption parameters

Isotherm models	Parameter	value
Langmuir	Qmax (mg g ⁻¹)	2
	KL (L mol ⁻¹)	1599100
	E (kJ mol ⁻¹)	35.392
Freundlich	R ²	1
	Kf (mg g ⁻¹)	1.351
	n	1
Temkin	R ²	1
	B	0.015
	A	5.5x1060
Harkin-Jura	R ²	0.868
	A	0.00944
	B	0.00572
Redelich-Peterson	R ²	0.701
	Kr (L g ⁻¹)	116.39
	β	20.66
Jovanovic	R ²	0.972
	Kj	55.05
	qmax (mg g ⁻¹)	4.56 x 10-46
Halsey	R ²	0.868
	n	1
	KH	1.609
	R ²	1

Table 6 provides the R^2 values for the isothermal adsorption models of Langmuir, Freundlich, Temkin, Harkin-Jura, Redlich-Peterson, Jovanovic, and Halsey. The isothermal adsorption models that exhibit the highest suitability for methylene blue (MB) adsorption onto TSAA, with R^2 values approaching 1, are Langmuir, Freundlich, and Halsey. The outcomes of this investigation imply that the adsorption of MB onto TSAA may proceed via a chemisorption⁶⁰ and physisorption mechanism³⁵. According to the Langmuir isotherm model, the adsorption process forms a monolayer of adsorbate on the adsorbent surface, where each active site on the adsorbent can accommodate only one adsorbate molecule. This is due to the equilibrium between the number of adsorbate molecules and the functional sites available on the adsorbent surface⁷⁷. This conclusion is supported by the data presented in **Figure 9**, which indicates that after 30 minutes, there was no additional increase in the amount of adsorbate adsorbed. Furthermore, after 30 minutes of adsorption, the conditions tend to decrease and remain constant. It is suspected that adsorbate release occurred because there is a possibility of physical adsorption occurring. According to theory, the Freundlich isotherm suggests that adsorbate molecules will form multiple layers on the surface of the adsorbent, indicating a multilayer adsorption process⁷⁸. This finding is further substantiated by the data in **Figure 2**, which reveals the presence of a porous biosorbent surface. Despite both the Langmuir and Freundlich isotherms yielding the same R^2 value, it is noteworthy that the Freundlich model's parameter n equals one. If the n value is

between 1 and 10, adsorption occurs according to the Freundlich isothermal ⁷⁹. It is known that the Kf value is 1,351 mg g⁻¹, meaning that by using 1 g of teak sawdust, 1,351 mg MB can be absorbed every 30 minutes of the adsorption process. Besides that, based on the data, the R² value for Halsey isothermal

adsorption is 1, which is the adsorption that occurs in a multilayer. Additionally, the R² value for the Temkin isotherm indicates that the distribution of the adsorbate across the adsorbent surface is uniform, suggesting the absence of multiple adsorbate layers ⁵⁶.

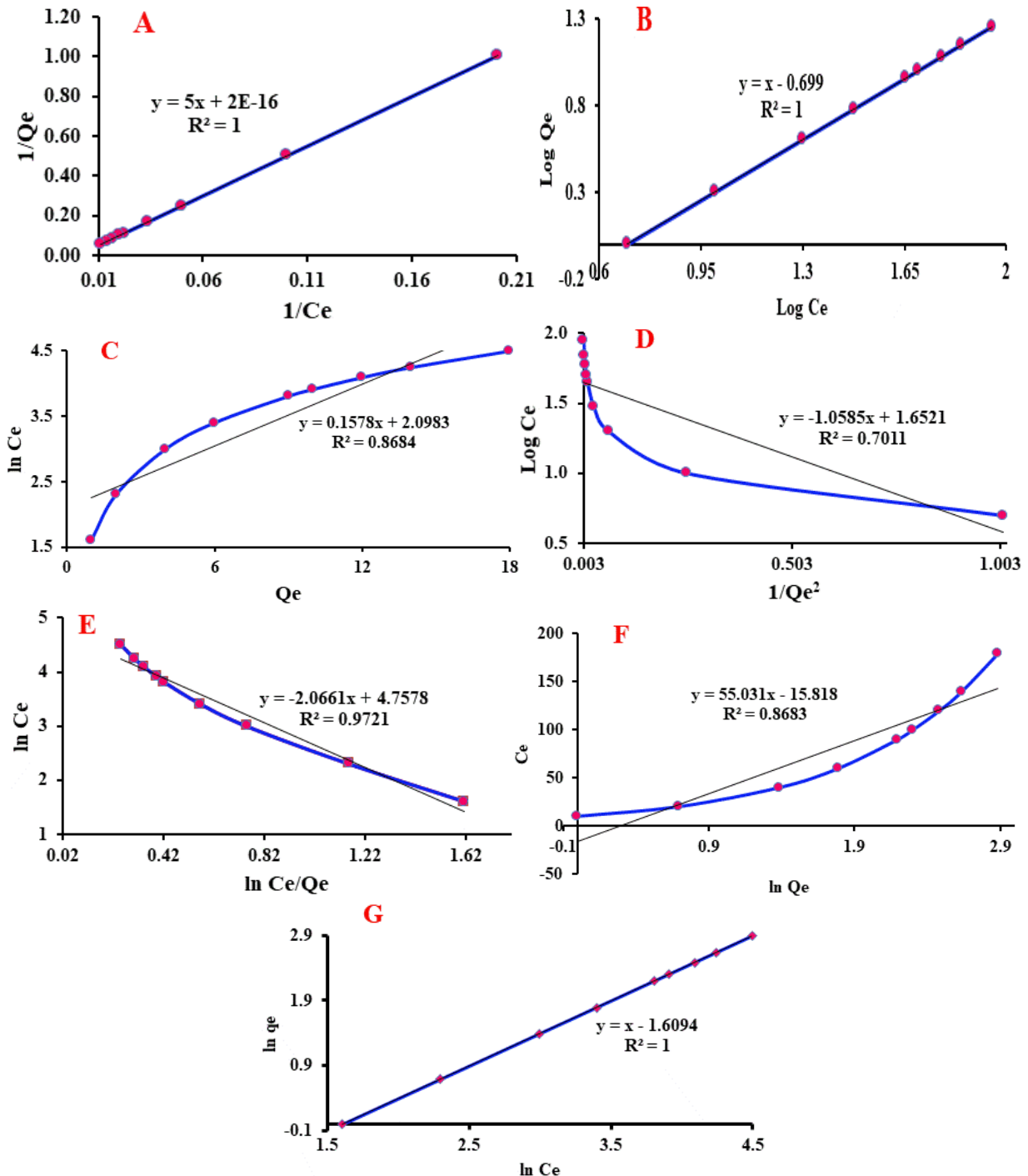


Figure 9. Adsorption isothermal graph plot: A) Langmuir; B) Freundlich; C) Temkin; D) Harkin–Jura; E) Redelich–Peterson; F) Jovacic; and G) Halsey

4. CONCLUSIONS

The research findings indicate that TSAA is an effective adsorbent for the cationic dye methylene blue. Optimal adsorption conditions were identified at a contact time of 30 minutes and a pH of 6. The kinetics adsorption is most accurately represented by a pseudo-second-order model, with a rate constant (K) of $79.71 \text{ g mg}^{-1} \text{ min}^{-1}$. Maximum adsorption capacity is observed at a methylene blue concentration of 30 ppm. Isothermal adsorption data align with the Freundlich and Halsey models, indicating a maximum adsorption capacity of 1.351 mg g^{-1} and an empirical constant n of 1. These results suggest that the adsorption process is characterized by multilayer coverage.

ACKNOWLEDGMENTS

This project was financially funded by the Research and Community Service Unit (LPPM) of Widya Mandira Catholic University under the Regular Research Grant 2023.

REFERENCES

- Desore A, Narula SA. An overview on corporate response towards sustainability issues in textile industry. *Environ Dev Sustain*. 2018;20(4):1439-1459. doi:10.1007/s10668-017-9949-1
- Zhu H, Chen S, Luo Y. Adsorption mechanisms of hydrogels for heavy metal and organic dyes removal: A short review. *Journal of Agriculture and Food Research*. 2023;12:100552. doi:10.1016/j.jafr.2023.100552
- Azis T, Ahmad LO, Rosa FE, Kadir LA. Study of Equilibrium and Kinetics of Pb(II) in Solution Using Persimmon Tannin Gel as an Adsorbent. *J Kim Sains Apl*. 2019;22(6):310-316. doi:10.14710/jksa.22.6.310-316
- Sountharajah D, Loganathan P, Kandasamy J, Vigneswaran S. Effects of Humic Acid and Suspended Solids on the Removal of Heavy Metals from Water by Adsorption onto Granular Activated Carbon. *IJERPH*. 2015;12(9):10475-10489. doi:10.3390/ijerph120910475
- Chong MY, Tam YJ. Bioremediation of dyes using coconut parts via adsorption: a review. *SN Appl Sci*. 2020;2(2):187. doi:10.1007/s42452-020-1978-y
- Oladoye PO, Ajiboye TO, Omotola EO, Oyewola OJ. Methylene blue dye: Toxicity and potential elimination technology from wastewater. *Results in Engineering*. 2022;16:100678. doi:10.1016/j.rineng.2022.100678
- Lellis B, Fávoro-Polonio CZ, Pamphile JA, Polonio JC. Effects of textile dyes on health and the environment and bioremediation potential of living organisms. *Biotechnology Research and Innovation*. 2019;3(2):275-290. doi:10.1016/j.biori.2019.09.001
- Afrin S, Shuvo HR, Sultana B, et al. The degradation of textile industry dyes using the effective bacterial consortium. *Heliyon*. 2021;7(10):e08102. doi:10.1016/j.heliyon.2021.e08102
- Zein R, Satrio Purnomo J, Ramadhani P, Safni, Alif MF, Putri CN. Enhancing sorption capacity of methylene blue dye using solid waste of lemongrass biosorbent by modification method. *Arabian Journal of Chemistry*. 2023;16(2):104480. doi:10.1016/j.arabjc.2022.104480
- Suresh S. Removal of Basic Violet 14 from aqueous solution using sulphuric acid activated materials. *SpringerPlus*. 2016;5(1):633. doi:10.1186/s40064-016-2294-2
- Handayani SN, Irmanto I, Indriyani NN. Determination of The Adsorption Kinetics for Adsorption Methylene Blue Dye with C-4-Hydroxy-3-Methoxyphenylcalix[4]resorcinarene. *Molekul*. 2023;18(1):107-116. doi:10.20884/1.jm.2023.18.1.6768
- Jumaeri J, Nadiyya A, Prasetya AT, Sumarni W. Congo Red Dye Adsorption using Magnesium Hydroxide from Seawater Bittern. *J Kim Sains Apl*. 2022;25(6):205-211. doi:10.14710/jksa.25.6.205-211
- Hardian A, Rosidah R, Budiman S, Syarif DG. Preparation of Composite Derived from Banana Peel Activated Carbon and MgFe_2O_4 as Magnetic Adsorbent for Methylene Blue Removal. *J Kim Sains Apl*. 2021;23(12):440-448. doi:10.14710/jksa.23.12.440-448
- Staroń P, Chwastowski J, Banach M. Sorption behavior of methylene blue from aqueous solution by raphia fibers. *Int J Environ Sci Technol*. 2019;16(12):8449-8460. doi:10.1007/s13762-019-02446-9
- Długosz O, Szostak K, Krupiński M, Banach M. Synthesis of $\text{Fe}_3\text{O}_4/\text{ZnO}$ nanoparticles and their application for the photodegradation of anionic and cationic dyes. *Int J Environ Sci Technol*. 2021;18(3):561-574. doi:10.1007/s13762-020-02852-4
- Kumar M S, N S, E D. Photocatalytic Degradation of Methylene Blue Using Silver Nanoparticles Synthesized from *Gymnema Sylvestre* and Antimicrobial Assay. *NRS*. 2019;2(2). doi:10.31031/NRS.2019.02.000532
- Talaiekhosravi A, Reza Mosayebi M, Fulazzaky MA, Eskandari Z, Sanayee R. Combination of TiO_2 microreactor and electroflotation for organic pollutant removal from textile dyeing industry wastewater. *Alexandria Engineering Journal*.

- 2020;59(2):549-563.
doi:10.1016/j.aej.2020.01.052
18. Riyanto, Mawazi M. Electrochemical Degradation of Methylene Blue Using Carbon Composite Electrode (C-PVC) in Sodium Chloride. *IOSR Journal of Applied Chemistry*. 2015;8(11):31-40. doi:10.9790/5736-081113140
 19. Azis T, Ahmad LO, Awaliyah K, Kadir LA. Study of Kinetics and Adsorption Isotherm of Methylene Blue Dye using Tannin Gel from Ceriops tagal. *J Kim Sains Apl*. 2020;23(10):370-376. doi:10.14710/jksa.23.10.370-376
 20. Al Ashik A, Rahman MdA, Halder D, Hossain MdM. Removal of methylene blue from aqueous solution by coconut coir dust as a low-cost adsorbent. *Appl Water Sci*. 2023;13(3):81. doi:10.1007/s13201-023-01887-5
 21. Rosanti AD, Kusumawati Y, HiDayat F, Fadlan A, Wardani AR k., Anggraeni HA. Adsorption of Methylene Blue and Methyl Orange from Aqueous Solution using Orange Peel and CTAB-Modified Orange Peel. *Journal of the Turkish Chemical Society Section A: Chemistry*. 2022;9(1):237-246. doi:10.18596/jotcsa.1003132
 22. Mittal H, Al Alili A, Alhassan SM. High efficiency removal of methylene blue dye using κ -carrageenan-poly(acrylamide-co-methacrylic acid)/AQSOA-Z05 zeolite hydrogel composites. *Cellulose*. 2020;27(14):8269-8285. doi:10.1007/s10570-020-03365-6
 23. Nipa ST, Shefa NR, Parvin S, et al. Adsorption of methylene blue on papaya bark fiber: Equilibrium, isotherm and kinetic perspectives. *Results in Engineering*. 2023;17:100857. doi:10.1016/j.rineng.2022.100857
 24. Utomo HD, Phoon RYN, Shen Z, Ng LH, Lim ZB. Removal of Methylene Blue Using Chemically Modified Sugarcane Bagasse. *Natural Resources*. 2015;6(4):209-220. doi:10.4236/nr.2015.64019
 25. Baunsele AB, Missa H. Kajian Kinetika Adsorpsi Metilen Biru Menggunakan Adsorben Sabut Kelapa. *Akta Kimia Indonesia*. 2020;5(2):76-85.
 26. Baunsele AB, Missa H. Langmuir and Freundlich Equation Test on Methylene Blue Adsorption by Using Coconut Fiber Biosorbent. *Walisongo Journal of Chemistry*. 2021;4(2):131-138. doi:10.21580/wjc.v4i2.8941
 27. Baunsele AB, Boelan EG, Kopon AM, Rahayu R, Siswanta D. Kinetic Study of Blue Methylene Adsorption Using Coconut Husk Base Activated. *I*. 2022;10(2):110-116. doi:10.30598/ijcr.2022.10-ans
 28. Baunsele AB, Boelan EG, Kopon AM, Taek MM, Tukan GD, Missa H. Penggunaan Sabut Kelapa Teraktivasi NaOH sebagai Adsorben Metilen Biru: *KOVALEN: Jurnal Riset Kimia*. 2023;9(1):43-54. doi:10.22487/kovalen.2023.v9.i1.16274
 29. Baunsele AB, Kopon AM, Boelan EG, et al. Adsorption of Methylene Blue using the Biosorbent of Coconut Fiber Activated by Nitric Acid. *molekul*. 2024;19(1):128. doi:10.20884/1.jm.2024.19.1.9443
 30. Ninu YD, Baunsele AB. Studi Adsorpsi Metilen Biru Menggunakan Biosorben Sabut Buah Siwalan Teraktivasi Kalium Hidroksida. *SPIN*. 2023;5(1):50-66. doi:10.20414/spin.v5i1.6807
 31. Banamtuan TE, Baunsele AB, Kopon AM. Studi Adsorpsi Metilen Biru Memanfaatkan Sabut Buah Lontar. *Jurnal Inovasi Teknik Kimia*. 2023;8(2):108-116. doi:10.31942/inteka.v8i2.8065
 32. Moniz L, Baunsele AB, Boelan EG, et al. Optimasi Adsorpsi Metilen Biru Memanfaatkan Sabut Buah Lontar Teraktivasi Asam. *CAKRA KIMIA (Indonesian E-Journal of Applied Chemistry)*. 2024;12(1):17-31.
 33. Sylvia N, Dewi R, Zulnazri Z, Setiawan H, Humaira D, Reza M. Optimization of Methylene Blue Dye Adsorption in Fixed Bed Column Packed with Tea Waste via Response Surface Methodology. *J Kim Sains Apl*. 2023;26(8):310-317. doi:10.14710/jksa.26.8.310-317
 34. Kusuma HS, Aigbe UO, Ukhurebor KE, et al. Biosorption of Methylene blue using clove leaves waste modified with sodium hydroxide. *Results in Chemistry*. 2023;5:100778. doi:10.1016/j.rechem.2023.100778
 35. Esmaeili H, Foroutan R. Adsorptive Behavior of Methylene Blue onto Sawdust of Sour Lemon, Date Palm, and Eucalyptus as Agricultural Wastes. *Journal of Dispersion Science and Technology*. 2019;40(7):990-999. doi:10.1080/01932691.2018.1489828
 36. Chen C, Fu Y, Yu L li, Li J, Li D qiang. Removal of methylene blue by seed-watermelon pulp-based low-cost adsorbent: Study of adsorption isotherms and kinetic models. *Journal of Dispersion Science and Technology*. 2017;38(8):1142-1146. doi:10.1080/01932691.2016.1225263
 37. Fang J, Gao B, Mosa A, Zhan L. Chemical activation of hickory and peanut hull hydrochars for removal of lead and methylene blue from aqueous solutions. *Chemical Speciation & Bioavailability*. 2017;29(1):197-204. doi:10.1080/09542299.2017.1403294
 38. Baunsele AB, Kopon AM, Boelan EG, et al. Pengaruh pH dan Waktu Kontak Terhadap Adsorpsi Metilen Biru Menggunakan Serbuk Gergaji Kayu Jati. *Alotrop*. 2024;8(1):1-11. doi:10.33369/alo.v8i1.32235
 39. Kurniasih D, Sari KE, Wijayanti WP. Kajian Peluang Alternatif Pengolahan Limbah Serbuk

- Gergaji di Sentra Industri Mebel Kelurahan Bukir. *Planning for Urban Region and Environment*. 2021;10(4):9-18.
40. El-Nemr MA, Yilmaz M, Ragab S, El Nemr A. Biochar-SO prepared from pea peels by dehydration with sulfuric acid improves the adsorption of Cr⁶⁺ from water. *Biomass Conv Bioref*. 2024;14(2):2601-2619. doi:10.1007/s13399-022-02378-4
 41. Kusuma HS, Aigbe UO, Ukhurebor KE, et al. Biosorption of Methylene blue using clove leaves waste modified with sodium hydroxide. *Results in Chemistry*. 2023;5:100778. doi:10.1016/j.rechem.2023.100778
 42. Asasian KN, Sharifian S, Kaghazchi T. Investigation of sulfuric acid-treated activated carbon properties. *Turk J Chem*. 2019;43(2):663-675. doi:10.3906/kim-1810-63
 43. Cundari L, Fanneza AL, Arisma NC. Characterization of Biosorbent from Musa acuminata balbisian Peel using FTIR Spectroscopy and Its Application to Cadmium (Cd) Removal: Effect of Activator Type, pH, and Biosorbent Ratio. *CHEMICA: Jurnal Teknik Kimia*. 2023;9(3):142. doi:10.26555/chemica.v9i3.23992
 44. Kamila EA, Abidin Z, Arief II, Trivadila. Synthesis, Characterization, Antibacterial Activity, and Potential Water Filter Application of Copper Oxide/Zeolite Composite. *mss*. 2023;27(3). doi:10.7454/mss.v27i3.1555
 45. Mishra Y. Adsorption Studies of Basic Dyes Onto Teak (Tectona Grandis) Leaf Powder. *Journal of Urban and Environmental Engineering*. 2015;9(9):102-108. doi:10.4090/juee.2015.v9n2.102108
 46. Su P, Wan Q, Yang Y, et al. Hydroxylation of electrolytic manganese anode slime with EDTA-2Na and its adsorption of methylene blue. *Separation and Purification Technology*. 2021;278:119526. doi:10.1016/j.seppur.2021.119526
 47. Bello OS, Lasisi BM, Adigun OJ, Ephraim V. Scavenging Rhodamine B dye using moringa oleifera seed pod. *Chemical Speciation & Bioavailability*. 2017;29(1):120-134. doi:10.1080/09542299.2017.1356694
 48. Baunsele AB, Missa H. Kajian Kinetika Adsorpsi Metilen Biru Menggunakan Adsorben Sabut Kelapa. *Akta Kimia Indonesia*. 2020;5(2):76. doi:10.12962/j25493736.v5i2.7791
 49. Firdaus MYM, Aziz A, Azmier Ahmad M. Conversion of teak wood waste into microwave-irradiated activated carbon for cationic methylene blue dye removal: Optimization and batch studies. *Arabian Journal of Chemistry*. 2022;15(9):104081. doi:10.1016/j.arabjc.2022.104081
 50. Parushuram N, Ranjana R, Harisha KS, et al. Silk fibroin and silk fibroin-gold nanoparticles nanocomposite films: sustainable adsorbents for methylene blue dye. *Journal of Dispersion Science and Technology*. 2022;43(8):1161-1176. doi:10.1080/01932691.2020.1848578
 51. Abbou B, Lebki Ri I, Ouaddari H, et al. Kinetic and thermodynamic study on adsorption of cadmium from aqueous solutions using natural clay. *Journal of the Turkish Chemical Society Section A: Chemistry*. 2021;8(2):677-692. doi:10.18596/jotcsa.882016
 52. Yakout AA, Shaker MA, Elwakeel KZ, Alshitari W. Lauryl sulfate@magnetic graphene oxide nanosorbent for fast methylene blue recovery from aqueous solutions. *Journal of Dispersion Science and Technology*. 2019;40(5):707-715. doi:10.1080/01932691.2018.1477604
 53. Neolaka YAB, Lawa Y, Naat JN, et al. The adsorption of Cr(VI) from water samples using graphene oxide-magnetic (GO-Fe₃O₄) synthesized from natural cellulose-based graphite (kusambi wood or Schleicheria oleosa): Study of kinetics, isotherms and thermodynamics. *Journal of Materials Research and Technology*. 2020;9(3):6544-6556. doi:10.1016/j.jmrt.2020.04.040
 54. Ahmad MA, Ahmed NB, Adegoke KA, Bello OS. Sorption studies of methyl red dye removal using lemon grass (Cymbopogon citratus). *Chemical Data Collections*. 2019;22:100249. doi:10.1016/j.cdc.2019.100249
 55. Ayawei N, Ebelegi AN, Wankasi D. Modelling and Interpretation of Adsorption Isotherms. *Journal of Chemistry*. 2017;2017. doi:10.1155/2017/3039817
 56. Ragadhita R, Nandiyanto ABD. How to Calculate Adsorption Isotherms of Particles Using Two-Parameter Monolayer Adsorption Models and Equations. *Indonesian J Sci Technol*. 2021;6(1):205-234. doi:10.17509/ijost.v6i1.32354
 57. Trisanti PN, Rifan M, Akbar P, Gunardi I, Sumarno S. Isolation of cellulose from teak wood using hydrothermal method. In: AIP Publishing; 2021:020047. doi:10.1063/5.0053874
 58. Hina K, Zou H, Qian W, Zuo D, Yi C. Preparation and performance comparison of cellulose-based activated carbon fibres. *Cellulose*. 2018;25(1):607-617. doi:10.1007/s10570-017-1560-y
 59. Gorgieva S, Vogrinčič R, Kokol V. The Effect of Membrane Structure Prepared from Carboxymethyl Cellulose and Cellulose Nanofibrils for Cationic Dye Removal. *J Polym*

- Environ.* 2019;27(2):318-332. doi:10.1007/s10924-018-1341-1
60. Acut E, Anorico NF, Acut D. Optimization of the Removal of Hexavalent Chromium Cr(VI) from Aqueous Solution by Moringa oleifera Bark-Derived Activated Carbon (MOBAC) Using Response Surface Methodology (RSM). *Orbital: Electron J Chem.* Published online December 29, 2023;186-197. doi:10.17807/orbital.v15i4.19352
 61. Nizam NUM, Hanafiah MM, Mahmoudi E, Halim AA, Mohammad AW. The removal of anionic and cationic dyes from an aqueous solution using biomass-based activated carbon. *Sci Rep.* 2021;11(1):8623. doi:10.1038/s41598-021-88084-z
 62. Ahmad MA, Ahmed NB, Adegoke KA, Bello OS. Sorption studies of methyl red dye removal using lemon grass (*Cymbopogon citratus*). *Chemical Data Collections.* 2019;22:100249. doi:10.1016/j.cdc.2019.100249
 63. Yildirim A, Acay H. Biosorption studies of mushrooms for two typical dyes. *Journal of the Turkish Chemical Society Section A: Chemistry.* 2020;7(1):295-306. doi:10.18596/jotcsa.581007
 64. Baunsele AB, Missa H. Langmuir and Freundlich Equation Test on Methylene Blue Adsorption by Using Coconut Fiber Biosorbent. *Walisongo Journal of Chemistry.* 2021;4(2):131-138.
 65. Grzabka-Zasadzińska A, Ratajczak I, Król K, Woźniak M, Borysiak S. The influence of crystalline structure of cellulose in chitosan-based biocomposites on removal of Ca(II), Mg(II), Fe(III) ion in aqueous solutions. *Cellulose.* 2021;28(9):5745-5759. doi:10.1007/s10570-021-03899-3
 66. Kamari A, Yusoff SNM, Abdullah F, Putra WP. Biosorptive removal of Cu(II), Ni(II) and Pb(II) ions from aqueous solutions using coconut dregs residue: Adsorption and characterisation studies. *Journal of Environmental Chemical Engineering.* 2014;2(4):1912-1919. doi:10.1016/j.jece.2014.08.014
 67. Pathania D, Sharma S, Singh P. Removal of methylene blue by adsorption onto activated carbon developed from *Ficus carica* bast. *Arabian Journal of Chemistry.* 2017;10:S1445-S1451. doi:10.1016/j.arabjc.2013.04.021
 68. Bello OS, Adegoke KA, Fagbenro SO, Lameed OS. Functionalized coconut husks for rhodamine-B dye sequestration. *Appl Water Sci.* 2019;9(8):189. doi:10.1007/s13201-019-1051-4
 69. Moirana RL, Mkunda J, Machunda R, Paradelo M, Mtei K. Hydroxyapatite-activated seaweed biochar for enhanced remediation of fluoride contaminated soil at various pH ranges. *Environmental Advances.* 2023;11:100329. doi:10.1016/j.envadv.2022.100329
 70. Bello OS, Adegoke KA, Fagbenro SO, Lameed OS. Functionalized coconut husks for rhodamine-B dye sequestration. *Appl Water Sci.* 2019;9(8):189. doi:10.1007/s13201-019-1051-4
 71. Al-Maliky EA, Gzar HA, Al-Azawy MG. Determination of Point of Zero Charge (PZC) of Concrete Particles Adsorbents. *IOP Conf Ser: Mater Sci Eng.* 2021;1184(1):012004. doi:10.1088/1757-899X/1184/1/012004
 72. Baunsele AB, Boelan EG, Kopon AM, Rahayu R, Siswanta D. Kinetic Study of Blue Methylene Adsorption Using Coconut Husk Base Activated. *Indo J Chem Res.* 2022;10(2):110-116. doi:10.30598/ijcr.2022.10-ans
 73. De Oliveira FM, Rodrigues De Sousa PA, De Melo EI, Coelho LM. Evaluation of the Adsorption Process Using Low Cost Agroindustry Residue for the Removal of Methylene Blue Dye. *Orbital: Electron J Chem.* 2020;12(2):76-86. doi:10.17807/orbital.v12i2.1422
 74. Fairouz AK, Mushtaq MAB, Arif PMA, Mazahar MF. A Comparative Study of Adsorption of Methylene Blue Dye onto Untreated *Platanus orientalis* (chinar tree) Leaves Powder and its Biochar - Equilibrium, Kinetic and Thermodynamic Study. *Orbital: Electron J Chem.* Published online October 11, 2023:163-170. doi:10.17807/orbital.v15i3.18358
 75. Gong L, Sun W, Kong L. Adsorption of Methylene Blue by NaOH-modified Dead Leaves of Plane Trees. *Computational Water, Energy, and Environmental Engineering.* 2013;2(2):13-19. doi:10.4236/cweee.2013.22B003
 76. Hameed BH, Mahmoud DK, Ahmad AL. Equilibrium modeling and kinetic studies on the adsorption of basic dye by a low-cost adsorbent: Coconut (*Cocos nucifera*) bunch waste. *Journal of Hazardous Materials.* 2008;158(1):65-72. doi:10.1016/j.jhazmat.2008.01.034
 77. El-Bery HM, Saleh M, El-Gendy RA, Saleh MR, Thabet SM. High adsorption capacity of phenol and methylene blue using activated carbon derived from lignocellulosic agriculture wastes. *Sci Rep.* 2022;12(1):5499. doi:10.1038/s41598-022-09475-4
 78. Campos AFC, Silva FND, Almeida MRBD, Sales LCA, Michels-Brito PH, Oliveira HALD. Thermodynamics of Cr(VI) Adsorption on Magnetic Core-Shell Nanoparticles. *Orbital: Electron J Chem.* 2019;11(2):64-70. doi:10.17807/orbital.v11i2.1331
 79. Jirekar D, Ubale M, Farooqui M. Evaluation of Adsorption Capacity of Low Cost Adsorbent for the Removal of Congo Red Dye from Aqueous Solution. *Orbital: Electron J Chem.* 2016;8(5):282-287. doi:10.17807/orbital.v8i5.834